Second flexural and torsional modes of vibration in suspended microfluidic resonator for liquid density measurements

Belardinelli, Pierpaolo; D Souza, Savio; Verlinden, Eleonoor; Wei, Jia; Staufer, Urs; Alijani, Farbod; Ghatkesar, Murali

DOI
10.1088/1361-6439/ab772c

Publication date
2020

Document Version
Final published version

Published in
Journal of Micromechanics and Microengineering

Journal of Micromechanics and Microengineering

Second flexural and torsional modes of vibration in suspended microfluidic resonator for liquid density measurements

OPEN ACCESS
IOP Publishing
Journal of Micromechanics and Microengineering
J. Micromech. Microeng. **30** (2020) 055003 (10pp)
https://doi.org/10.1088/1361-6439/ab772c

Second flexural and torsional modes of vibration in suspended microfluidic resonator for liquid density measurements

Pierpaolo Belardinelli[1,3], Savio N F D Souza[1], Eleonoor Verlinden[1], Jia Wei[2], Urs Staufer[1], Farbod Alijani[1] and Murali K Ghatkesar[1]

[1] Department of Precision and Microsystems Engineering, 3ME, Mekelweg 2, (2628 CD) Delft, The Netherlands
[2] Department of Microelectronics, EEMC, Mekelweg 4, (2628 CD) Delft, The Netherlands

E-mail: f.alijani@tudelft.nl and m.k.ghatkesar@tudelft.nl

Received 2 December 2019, revised 20 January 2020
Accepted for publication 17 February 2020
Published 6 April 2020

Abstract

Suspended microfluidic resonators enable detection of fluid density and viscosity with high sensitivity. Here, a two-legged suspended microchannel resonator that probes pico-litres of liquid is presented. The higher resonant modes (flexural and torsional) were explored for increased sensitivity and resolution. Unlike other reported microchannel resonators, this device showed an increase in the quality factor with resonant frequency value. The performance of the resonator was tested by filling the channel with three liquids, one at a time, over a density range of 779−1110 kg m^{-3} and a viscosity range of 0.89−16.2 mPa s. The highest resolution obtained was 0.011% change in density. Measurements with torsional mode showed an improvement of about six times in sensitivity and about fifteen times in resolution compared to the first flexural mode. When the empty channel was filled with liquids of different viscosity, the quality factor of the first flexural mode remained overall constant with a variation below 3.3% between the fluids, and confirming the inherent property of suspended microchannel resonators. However, it significantly decreased for second flexural and torsional modes. No noticeable difference was observed in the quality factor between different liquid viscosities for all modes.

Keywords: suspended microchannel resonator, microfluidic cantilever, hollow microcantilever, resonance frequency, quality factor, density measurement

(Some figures may appear in colour only in the online journal)

1. Introduction

The ability to accurately measure density in small volumes is crucial in variety of fields, e.g. biomedical research [1], chemical industry [2] and petroleum applications [3]. For large volumes (>1 ml), density is typically measured by weighting a known volume of liquid. The viscosity can be obtained by capillary viscometry or by falling sphere inside the liquid [4]. For volumes around 1 ml, resonant based techniques, where change in the resonant frequency as a function of liquid density can be used, like vibrating glass tubes [5], surface acoustic waves [6, 7], tuning forks [8], quartz crystal microbalance [9] or thin film bulk acoustic waves [10]. For volumes around 1 μl, again resonant based methods that use microtube resonators [11], microcantilever resonators immersed in liquid [12]

[1] Current affiliation: DICEA, Polytechnic University of Marche, Ancona, Italy

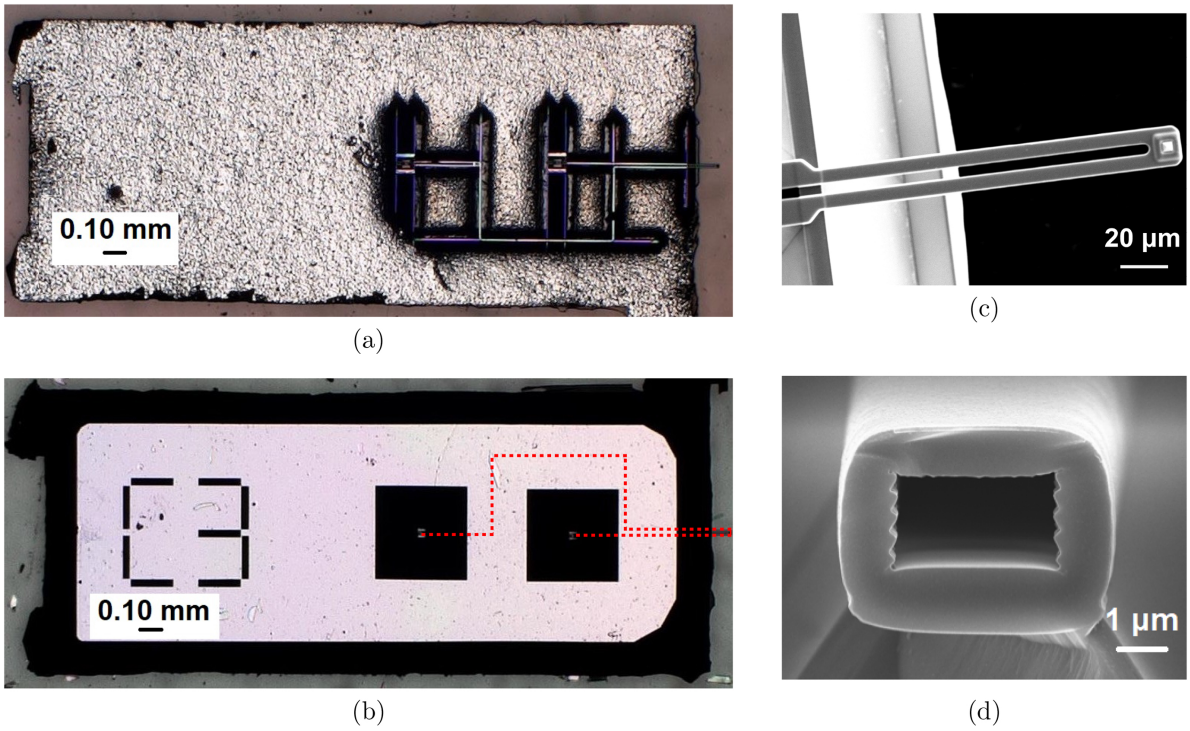

Figure 1. The microfluidic cantilever chip. (a) An optical image of the chip with a microfluidic network on the chip. The suspended microfluidic cantilever is at the middle of the right-side edge. (b) An optical image of the back side of chip with two reservoirs. The red dashed lines highlight the fluidic path to/from the reservoirs. (c) The scanning electron microscopy image of the hollow cantilever. (d) The cross-section of the fluid channel embedded in the cantilever [20, 21]. Reprinted from [20], Copyright (2017), with permission from Elsevier.

Table 1. Device details and dimensions.

Parameter	Value in μm
Cantilever length	155.0
Cantilever width	16.0
Cantilever height	4.9
Cantilever leg width	5.0
Gap between the two legs	6.0
Fluid channel height	2.2
Fluid channel width	3.7
Chip length	3030
Chip width	1100
Chip height	250

or microtube resonators experiencing Coriolis force [13, 14] can be used. The vibrating signals are highly damped [15] if the sensor is immersed inside the liquid, significantly effecting the sensitivity [16]. However, by flowing liquid through the sensor, vibration damping can be significantly reduced and the sensitivity can be improved [17]. The energy dissipation in the vibrating structures typically is a function of viscosity, thus enabling to simultaneously obtain density and viscosity of a liquid by monitoring frequency shift and quality factor respectively.

Here, we use a microfluidic cantilever based resonant sensor which uses only picolitre (pl) volumes of liquid. The fluid was flown through the channel inside the cantilever. The cantilever itself was operated in vacuum, thus removing also air damping on the resonant sensor. Such suspended microchannel resonators were used earlier to measure density and viscosity of fluids [18, 19]. However, higher resonant modes were not investigated in such devices to monitor fluid properties. We address that aspect in this work.

The device used for the measurement is a two-legged microfluidic cantilever. The unique aspects of the device are: it is made out of transparent silicon dioxide, uses only 12 pl of volume in the sensing region, and the chip size is made to fit in any commercial atomic force microscope (AFM) setup. The first two flexural modes and the first torsional mode of vibration were measured and analyzed.

2. Device Details

Hollow cantilevers were fabricated using a process originally described elsewhere [22, 23]. The fabrication method involved three main steps: i) two silicon wafers with fluid reservoir etched in the top wafer and cantilever channels etched in the bottom wafer were bonded together; ii) the channels and the reservoir were oxidized; iii) the bottom wafer was selectively etched to form on-chip channels and a suspended hollow cantilever, all made out of silicon dioxide. Simultaneously, the perimeter of the chip was etched and made to attach over breaking beams with the wafer. Finally, individual microfluidic cantilever chips were released from the wafer by applying a gentle manual pressure.

The microfluidic chip with fluidic network and the suspended cantilever is shown in figure 1(a) [22]. The cantilever is connected through on-chip microfluidic channel

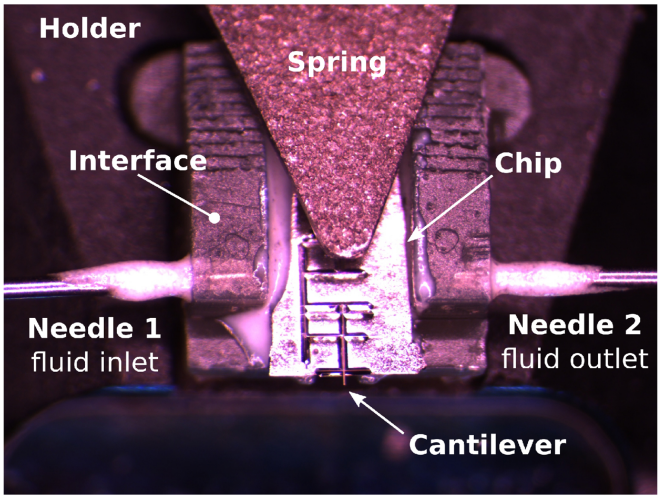

Figure 2. Chip glued to a 3D printed plastic fluidic interface that had two needles glued on either side for the fluid inlet and outlet. The entire assembly was mounted on a Nanosurf cantilever holder and clamped with a spring.

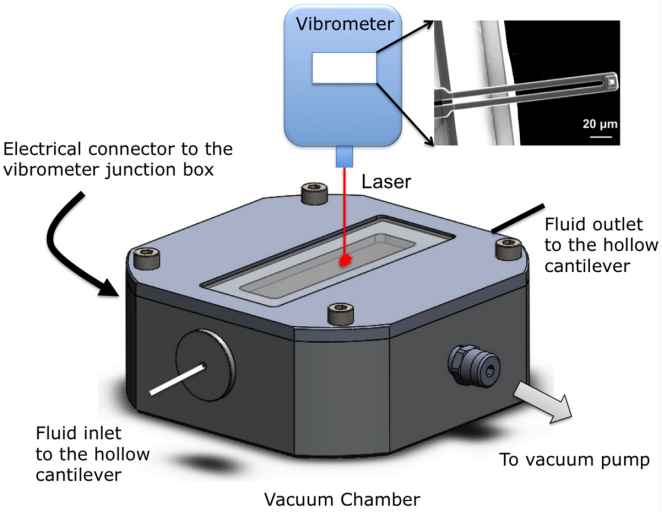

Figure 3. The measurement setup. The chip was mounted inside the vacuum chamber that had four connecting ports: two fluidic, a vacuum and an electrical. The transparent glass slide on the top was an optical window for the vibrometer, both to view and measure resonance of the cantilever with the laser.

network to two reservoirs on the chip, see figure 1(b). These reservoirs were used as interface with the external world. They were used as inlet and outlet or vice-versa. The dotted lines in the figure indicate the microfluidic channel located on the other side of the chip. The cantilever and the on-chip channels were made out of silicon dioxide. The cantilever had two physically separated channels connected near the free end (figure 1(c)). There was also a hollow pyramidal tip (without any aperture) at the free end, which had no function for the results described in this work. The cross-section of the fluid channel is shown in figure 1(d). The dimensions of the hollow cantilever and the chip are given in table 1.

2.1. Fluidic interface

The fluid entered through one of the reservoir (450 μm $\times$ 450 μm), flowed through the on-chip fluid channel, suspended cantilever and exited from the other reservoir. The on-chip reservoirs were able to continuously exchange fluids with the macro world through a fluidic interface. The plastic interface was fabricated by a 3D printer with 25 μm resolution (EnvisionTEC Micro Plus HD) using acrylic resins. The reservoirs on the chip were precisely aligned to the reservoirs on the interface before they were glued together. The chip glued to the fluidic interface is shown in figure 2. Two disposable stainless steel needle tubes (Nordson, 32GA needles) were glued to the plastic fluidic interface. Their free ends were connected to Tygon tubing which had an inner and outer diameter of 0.25 mm and 1 mm, respectively. The fluids were injected from the external world into the hollow cantilever through the tygon tube.

3. Modal analysis/vibration testing

3.1. Experimental setup

The resonator chip glued to the plastic fluidic interface was mounted on a standard atomic force microscopy cantilever-holder from Nanosurf AG, where excitation piezo was mounted close to the cantilever chip location. The holder was placed in a small vacuum chamber in order to reduce damping by air and increase the quality factor. The chamber had fluid feed-throughs to inject or aspirate fluids, electrical feedthrough to excite the piezo and gas feed-through to evacuate air. The schematic of the setup with various components is shown in figure 3. The connection between chamber and vacuum pump also accommodated a leak valve to control the pressure inside the chamber and a Pirani gauge for pressure readout. A glass window on the vacuum chamber provided the optical access to the cantilever. A laser Doppler vibrometer (Polytec MSA-400-PM2-D) was used to monitor the resonance frequencies and evaluate quality factors. Using the built-in microscope of the vibrometer, the laser was positioned at the desired location on the cantilever.

3.2. Device characterization

To ensure proper reflection of the laser from the transparent surface of silicon dioxide, the chip was coated with 6 nm of Au/Pd. The excitation was provided in the linear cantilever vibration regime by employing wave excitation from the base. The force signal used in the experiments were of pseudo-random type. This excitation eliminated the leakage problem that a random excitation commonly encounters. The signal was a stationary ergodic, with random amplitude and phase distribution. The alignment grooves on the holder ensured reproducible clamping for multiple experiments. The resonance frequency and quality factor were extracted from the frequency–amplitude response in a linear regime. The quality factor was obtained from the frequency–amplitude response by fitting a Lorentzian and using peak frequency and full width at half maxima. The resonant frequencies and corresponding quality factor values in vacuum are given in

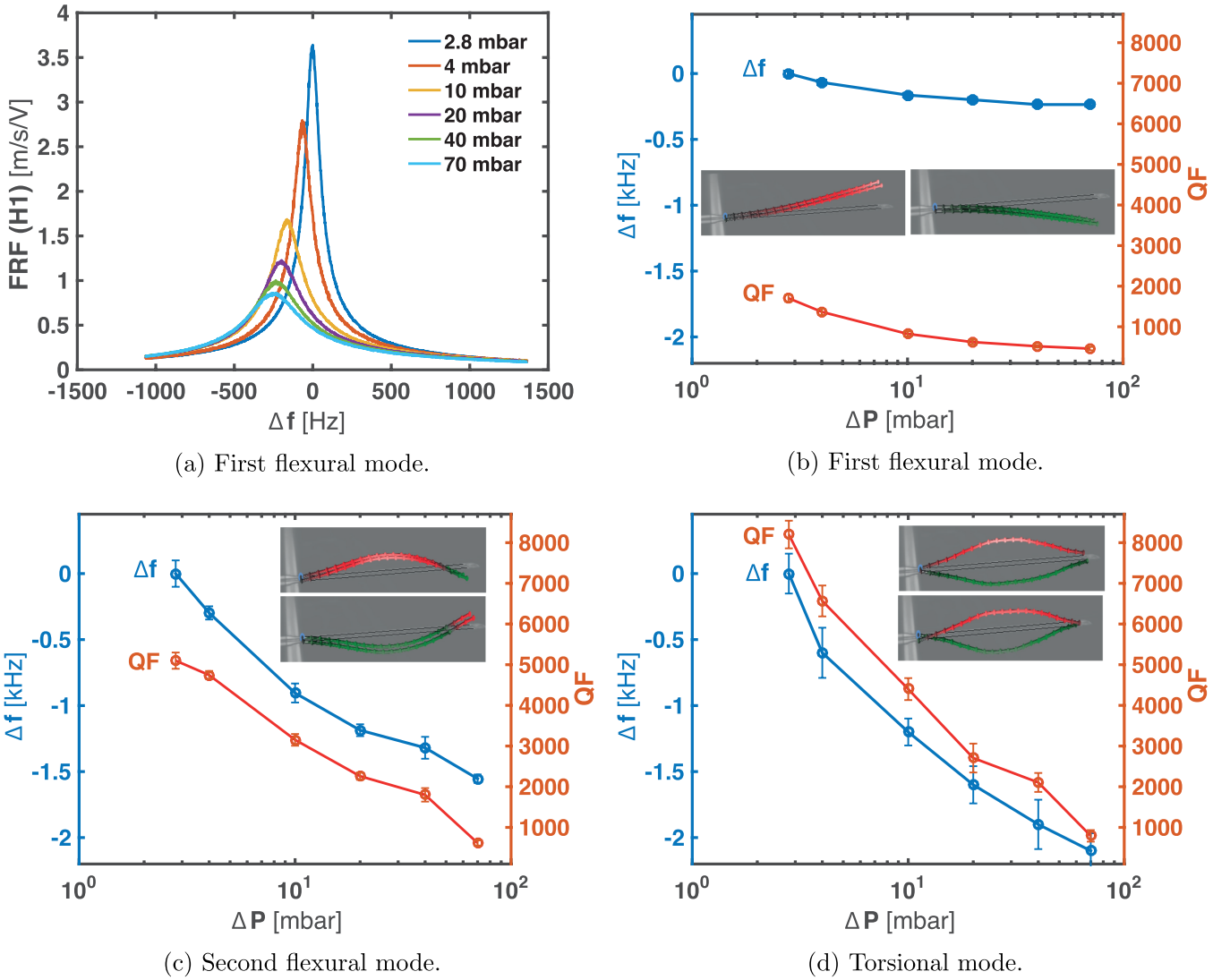

(a) First flexural mode.

(b) First flexural mode.

(c) Second flexural mode.

(d) Torsional mode.

Figure 4. Effect of air pressure on the resonant frequency and quality factor of various modes. The cantilever channel was filled with air, while the surrounding air was evacuated. (a) The increase in amplitude of the frequency response function (FRF) at different chamber pressures, (b)–(d) resonance frequency shifts (in blue) and quality factors (in red) as a function of pressure in the chamber (note: all baseline frequency values were taken at 2.8 mbar pressure in the chamber). The mode shapes computed via the Polytec Micro System Analyzer software are shown as the inset.

figure 4. In order to identify the different modes of vibration, we performed a full scan of the device by choosing a grid over the entire device. The points that composed the grid were scanned and measured. The grid points are visible as dots in the inset pictures of figure 4.

The fundamental frequency of this device, in air, was measured to be 134.53 kHz. The second flexural and the first torsional modes have also been obtained and their resonance frequencies were 828.25 kHz and 916.67 kHz, respectively.

The cantilever channels were filled with air, while the surrounding air outside the device was evacuated until 2.8 mbar (with mean free path of 36.75 μm)[4]. As a vacuum developed in the chamber, the resonance frequency for the first flexural mode of the device increased as shown in figure 4(a), 4(b). This increase was more prominent for the second mode (figure 4(c)). A similar trend was observed for the torsional (twisting) mode as shown in figure 4(d). This was consistent with the definition of the damped resonant frequency [25]:

$$\omega_d = \omega_n \sqrt{1 - 2\tau^2}, \tag{1}$$

where ω_n is the natural frequency and $\tau = 1/(2Q)$ is the damping ratio. As the pressure decreases, the damping ratio reduces and the resonant frequency increases as shown in figure 4(a).

When the effect of air damping was lowered, at 2.8 mbar, the quality factor for the first flexural mode improved to 1700 ($\approx$ 10 times increase) and to 5200 and 8200 for the second flexural and first torsional mode, respectively ($\approx$ 20 times increase from air). Note that the quality factor has not yet saturated indicating that it can be improved by further reducing the pressure level [26, 27].

[4] The mean free path was calculated considering effective cross-section for collision of air molecules of 2.82743×10^{-19} m^2 at $T = 298$ K [24].

Table 2. Density and dynamic viscosity of the characterized fluids at 20 °C (Data obtained from Material Safety Data Sheets).

Fluid	Density in kg m^{-3}	Viscosity in mPa s^{-1}
Air	1.204	0.018
Water	1000	0.890
Ethanol	779	1.100
Ethylene Glycol	1110	16.200

3.3. Density measurement using higher modes

After the modal testing of the microfluidic cantilever in air and vacuum, the cantilever was filled with three liquids of different density and viscosity. According to Khan *et al* [19], the shift in the inverse square of the resonant frequency (ω_n) is directly proportional to fluid density (ρ) changes inside the microfluidic cantilever. Mathematically, this can be expressed as:

$$\rho = \left(\frac{A}{\omega_n}\right)^2 - B, \tag{2}$$

where A and B are constants that can be determined by conducting experiments with two fluids of known densities. The three fluids along with their viscosities and densities at 20 °C are tabulated in table 2. All experiments were performed at room temperature, 20.25 ± 0.25 °C.

The fluids were injected/aspirated through the microfluidic cantilever using a syringe pump (Legato from KD Scientific) with a flow rate of 5 μl/min. Note that the volume inside the resonant probe region is only 12 pl. However, the connecting tube, device interface and the on-chip reservoir together require about 100 μl volume of fluid. To ensure complete exchange of liquids inside the channel, they were injected for about 3–4 min at the rate of 5 μl/min. The measurements were conducted after 10 min to ensure everything was stabilized. For the viscous ethylene glycol (about 16 times more viscous than water), an additional syringe pump withdrawing the fluid from outlet reservoir at a rate of 5 μl/min was used along with injection at the same rate from the inlet reservoir. After every experiment, the channels were rinsed with water.

The fluid flow in microfluidic channels was laminar. The Reynolds' number of the fluid in our device varied from 0.26 (air/first mode) to 31.2 (ethanol/torsional mode). All the values for various liquids and modes of vibration are listed in table A2 in the appendix (B).

4. Results and discussion

All the results were obtained with cantilever mounted inside the chamber. The chamber was evacuated to a pressure of 2.8 mbar. The channels of the cantilever were either empty (i.e. filled with air) or filled with water, ethanol or ethylene glycol.

4.1. Effect of vacuum outside hollow cantilever

The characterization of the empty hollow cantilevers in vacuum showed an improvement in quality factor of about an order of magnitude compared to air (see table 3). The quality factor of the first mode was approximately 15 times lower compared to the quality factor report by Khan *et al* [19]. However, their devices were operated at a pressure 10^5 times lower than the pressures of our setup. The sensors used by Lee *et al* [28] had 8 times higher quality factor for the first mode in high vacuum than our device. Their reported value of 8000 for first mode is close to the first torsional mode of our device.

Table 3. Comparison of quality factors in ambient and at 2.8 mbar.

Mode	Q in ambient	Q at 2.8 mbar
First flexural	150	1700
Second flexural	320	5200
First torsional	400	8200

The short term frequency stability of our device was tested by repeated measurements of the resonance peak at time intervals of one minute. The measured resonance frequencies for different modes are plotted in figure 5 as function of time and in terms of probability distribution. From the histogram plots and the fitted probability distribution we document the improved stability for the second flexural and first torsional mode. This confirms that density can be estimated more accurately at higher modes provided sensitivity is also higher at those modes [29]. Note that we did not had any temperature control for our sensors (temperature of the clean room was maintained at 20.25 ± 0.25 °C).

4.2. Effect of fluid density on frequency

Upon filling the microfluidic cantilever with a particular fluid, the flow was stopped and the measurements were made. The resonance frequency decreased corresponding to the increase in density of the fluid. The frequency shift obtained for three different liquids for the first flexural mode is shown in figure 6. The normalized amplitude response and the corresponding phase as function of the excitation frequency is plotted. The position of the laser probe on the cantilever is indicated in the inset. Even though this position was not optimal for analyzing the torsional mode, there was a sufficient signal level. The effect of fluid density on frequency for the higher modes is reported in appendix (A).

The resonance frequency shift as function of the fluid density for all modes is shown in figure 7. For each fluid we performed three experiments, the values for all the frequency shifts and the calculated standard deviation are reported in appendix (C).

We did not observe significant difference in the experimental results for repeated filling and emptying of the channels. The results were found perfectly reproducible.

There was a good linear fit (dashed lines) with Pearson's correlation coefficient of −0.99986, −0.99934, −0.99978 for the first, second and torsional mode respectively. In figure 7 solid red lines represent the fit according to equation (2). The coefficients A and B are calibrated by measuring the resonance frequency when filled with glycol and air. The values

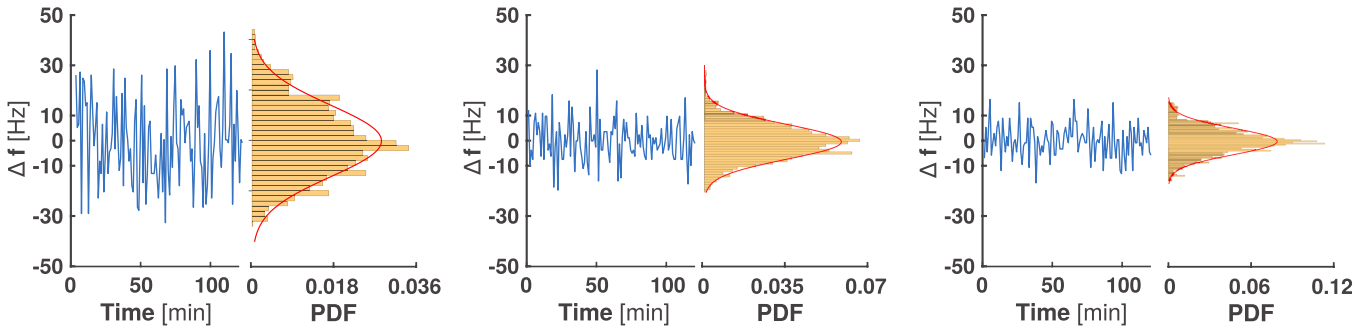

Figure 5. Stability of the resonant frequency measurement over two hours for the three modes. The two sub plots for each mode shown are the frequency stability in time and the fitted probability density function respectively. For the histogram the bins number was 50. (a) first flexural: mean value −0.212 145 Hz, standard deviation 14.2278 Hz; (b) second flexural: mean value −0.115 879 Hz, standard deviation 6.817 25 Hz; (c) first torsional mean value −0.343 445 Hz, standard deviation 5.495 34 Hz.

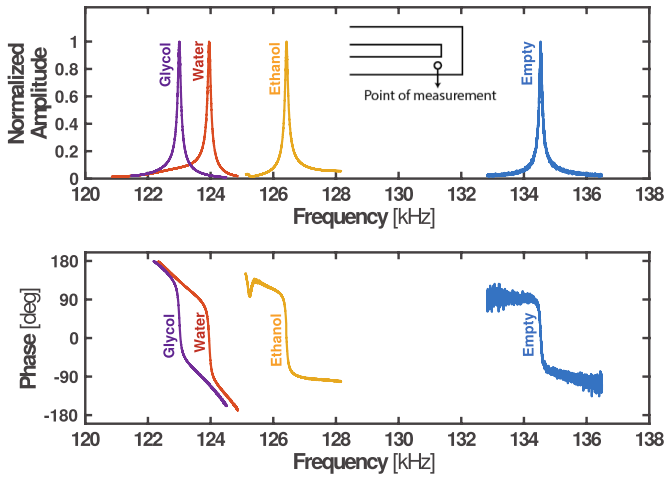

Figure 6. Normalized amplitude and phase responses near the resonance frequency of the first flexural mode for the empty hollow cantilever (blue) and the hollow cantilever filled with water (red), ethanol (yellow), and glycol (purple) at room temperature. The laser position point of measurement is indicated in the inset.

for the sensitivity derived from these plots are summarized in table 4. It is evident that higher mode measurements showed an increase in sensitivity with simultaneous improvement in the resolution. The change in density that was detectable using the first torsional mode (0.011%) in pl volume was better than the value of 0.06% in 5 μl volume that was detected using Mode 17 of cantilevers immersed in liquid [16]. The sensitivity levels of 57 Hz (kg m^{-3})$^{-1}$ in torsional mode and 63.01 Hz (kg m^{-3})$^{-1}$ for the second flexural mode was 3.6 times and 3.9 times higher respectively compared to 16.3 Hz (kg m^{-3})$^{-1}$ reported by Khan *et al* [19], where they monitored only fundamental mode during their measurements. Therefore, monitoring higher modes appear to increase the sensitivity in our device. The measurement system, i.e. laser spot, had no influence in the frequency shift for the filled cantilever. The results were reproducible for next few days. However, a slight change in the frequency was observed if the cantilever was removed and re-positioned. It was due to the irreproducible clamping condition.

4.3. Effect of viscosity on the quality factor

The energy dissipation in the microfluidic resonator is a combination of several components of loss that are in general challenging to disentangle [30, 31]. To simplify the dissipation in our system, we used the following equation:

$$\frac{1}{Q_{total}} = \frac{1}{Q_{fluid}} + \frac{1}{Q_{empty}}, \tag{3}$$

where Q_{total} is the overall effective quality factor, Q_{empty} is the quality factor of an empty (channels filled with ambient air) hollow cantilever vibrating in vacuum with all the dissipation factors (like clamping, intrinsic losses, etc) and Q_{fluid} is the dissipation factor due to fluid inside the channel. The quality factors obtained experimentally for all the modes when channels are filled with different fluids are given in table 5. The parameter Q_{total} is the experimentally measured value and Q_{fluid} is the value calculated from equation (3). The total quality factor Q_{total} for different liquids measured at different modes is plotted in figure 8.

There are several observations from the data. a) Q_{total} increased for second flexural and torsional mode compared to first flexural mode. b) Q_{fluid} decreased for second flexural and torsional mode compared to first flexural mode. c) Q_{total} was almost independent of fluid inside the channel for the first flexural mode. The variation between fluids was less than 3.3%. The small variation of the quality factor between fluids with different viscosities is within the framework of the non-monotonic variation predicted in Burg *et al* [32] d) Q_{total} for the second flexural and torsional mode significantly decreased when the empty channels were filled with liquids. The decrease from air to water was of 19%, 66% and 75% for the first, second flexural and torsional mode, respectively. e) Once filled with liquids, Q_{total} did not change significantly for different liquids and modes. The maximum variation was when filled with Glycol with a ΔQ_{total} of 360 (see second and

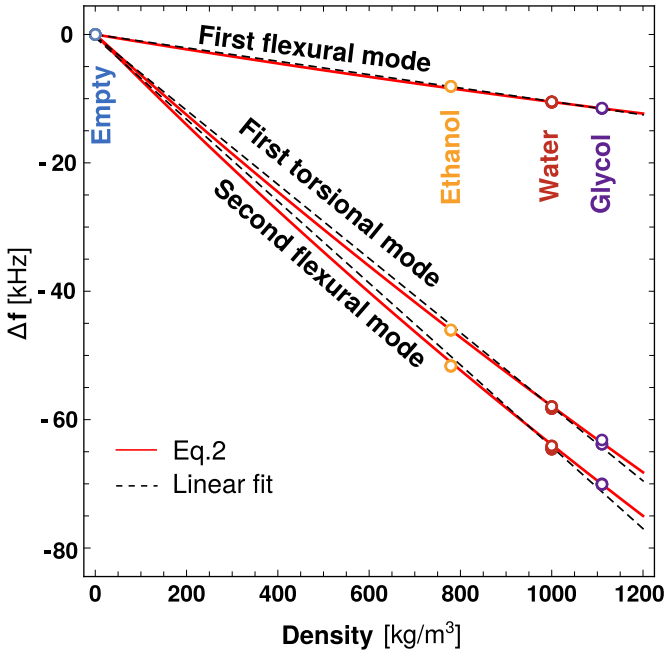

Figure 7. Frequency shifts of the first flexural mode (purple), second flexural mode (red) and first torsional mode (brown) with density of the fluid inside the hollow cantilever. The reading of the device when it is empty (filled with air) is taken as the baseline reading for all three modes (0 Hz). The black dashed line represents a linear fit. The red line is the calibration fit of equation (2). The coefficients A and B are: $\{A, B\} = \{10126.2, 5665.67\}$, $\{62874.4, 5748.77\}$, $\{77651.7, 7175.83\}$ for the first, second and torsional mode respectively.

Table 4. Sensitivity and stability of signal of various modes.

Mode	Sensitivity Hz (kg m^{-3})$^{-1}$	Stability of signal in Hz	Stability of signal in kg m^{-3}
First	10.49	16.6	1.58
Second	63.01	8.2	0.13
Torsional	57.16	6.4	0.11

third column of table 5). f) We observed a standard deviation of Q_{total} for ethanol for first flexural mode to be an order of magnitude lower with respect to other liquids. We could not explain this phenomenon and needs additional investigation.

The analytical equations to estimate Q_{fluid} for hollow cantilever filled with fluid was derived by Sader *et al* [33]. The calculated numbers are reported in appendix B. As predicted by the theory, Q_{fluid} of our device decreased at second flexural mode. This means the energy dissipation contribution from fluid is higher at the second flexural mode compared to the first flexural mode. This is attributed to the enhancement of the fluid compressibility at higher modes [33]. Additionally, due to fabrication limitations in producing perfectly symmetric devices along the channel height, the effective center position of the beam could be slightly off-axis. This results in net axial strain being experienced by the fluidic channel as the beam vibrates, leading to pumping of fluid inside the channel. This leads to additional acoustic effects contributing to damping. Interestingly, the Q_{fluid} for first torsional

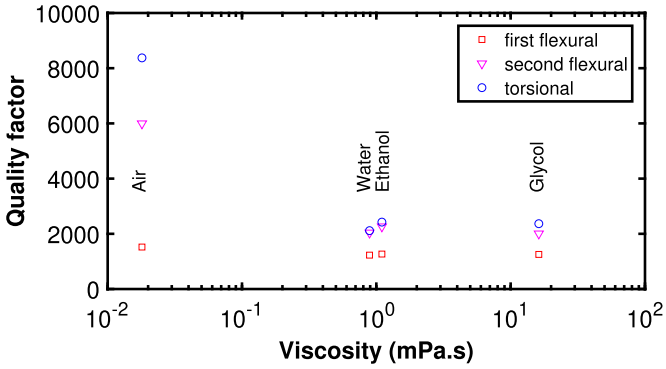

Figure 8. Change in the measured total quality factor at various modes with viscosity of liquids used in the experiments.

mode also shows higher dissipation than first flexural mode. Here, the legs are vibrating out of phase which can create additional fluid velocity gradients contributing to energy dissipation.

Even though Q_{fluid} seem to predict as estimated by the theory, the interesting part is the Q_{total} for our device. The measured Q_{total} increased for second flexural and torsional mode irrespective of the fluid, however, it was significantly higher for empty cantilever. This indicates that overall energy dissipation is lower at higher modes despite higher damping due to Q_{fluid} at higher resonant modes due to fluid. The energy dissipation due to effective inertia from device is dominating compared to viscous effects at higher modes. This is in contrast to the observations made by others [33, 34] and this could be either due to insufficient vacuum level outside the cantilever or the unique device geometry. The mean-free-path of air molecules, 36.75 μm at 2.8 mbar vacuum, is comparable to the dimensions of the cantilever, thus perhaps molecular viscosity of air is still playing a role. It is also known that quality factor increases with mode number in ambient air [29]. The geometry of our device is different from that used by Sader *et al* [34]. Our device has two channels physically separated (two legged), whereas their channels were physically attached as a single cantilever.

The Q_{total} of fundamental mode was almost independent of the liquid that was filled. This indicates that device inertial dissipation is very dominant over liquid viscous dissipation even over two orders in magnitude change in viscosity of fluid inside the channel. From theory, a non-monotonic behaviour of energy dissipation due to viscosity change was anticipated [32].

Overall, the total energy dissipation in our device is inertial dominated at higher frequency modes including torsional mode. The dissipation due to fluid has increased with higher frequency modes as predicted by theory, but overall still the inertial dissipation dominates. Further experiments would be to increase the vacuum level until the quality factor saturates and investigate the liquid damping behaviour of the device.

Table 5. Quality factors for the first two flexural and the first torsional mode when the microfluidic cantilever is empty and filled with ethanol, water and glycol. The standard deviation (SD) is given in the parenthesis. The Q_{fluid} for air is orders of magnitude higher.

	First Flexural Experiment		Second Flexural Experiment		First Torsional Experiment	
Fluid	Q_{total} (SD)	Q_{fluid}	Q_{total} (SD)	Q_{fluid}	Q_{total} (SD)	Q_{fluid}
Air	1 521.67 (22.54)	—	5 995.00 (9.16)	—	8 374.33 (6.02)	—
Ethanol	1 267.67 (2.52)	7 594.39	2 263.01 (58.88)	3 635.26	2 424.33 (58.31)	3 412.12
Water	1 228.33 (23.35)	6 371.83	2 037.67 (86.38)	3 086.89	2 115.66 (78.54)	2 830.83
Glycol	1 254.33 (24.44)	7 139.51	2 006.66 (93.38)	3 016.27	2 367.04 (130.28)	3 299.72

5. Conclusion

In this work, we present a physically separated two-legged hollow cantilever device. It has a quality factor of about 1700 for the first flexural mode of vibration at 2.8 mbar surrounding pressure. These quality factors are found to increase with mode number. For the first time, torsional mode in hollow cantilevers is measured. The first torsional mode exhibits a quality factor of about 8200, which is comparable to the quality factor of devices used in state-of-the-art cantilever based mass sensing applications. When the pl volume channels were filled with different liquids, resonance frequency shift increased with mode number for two flexural modes and the torsional mode. The respective sensitivities in density measurement for the three modes were 10.49 Hz (kg m^{-3})$^{-1}$, 63.01 Hz (kg m^{-3})$^{-1}$ and 57.16 Hz (kg m^{-3})$^{-1}$, respectively. There is also an improvement in resolution from 1.58 kg m^{-3} to 0.11 kg m^{-3} at higher modes of vibration which make the latter more attractive for sensing. The quality factor decreased when the channels were filled with liquid. However, there was not much change in the quality factor for different liquids at all modes. Furthermore, the quality factor increased for second flexural, which is contrary to the observations of others. The torsional mode had higher quality factor than flexural mode.

Acknowledgment

This work is part of the research project titled NFP4CryoEM with Project Number 13711, which is (partly) financed by the Netherlands Organisation for Scientific Research (NWO-TTW).

Appendix

Appendix A. Effect of fluid density on frequency for the higher modes

Figures A1 and A2 show the normalized amplitude and phase for the higher modes of vibration.

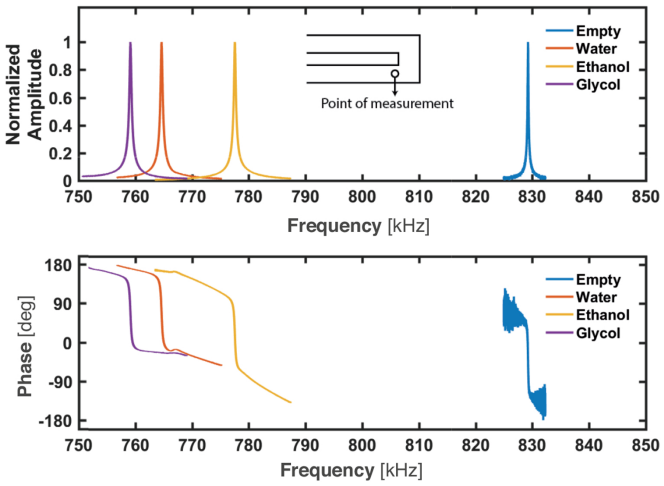

Figure A1. Normalized amplitude and phase (in degrees) responses near the resonance frequency of the second flexural mode for the empty hollow cantilever (blue) and the hollow cantilever filled with water (red), ethanol (yellow), and glycol (purple) at room temperature.

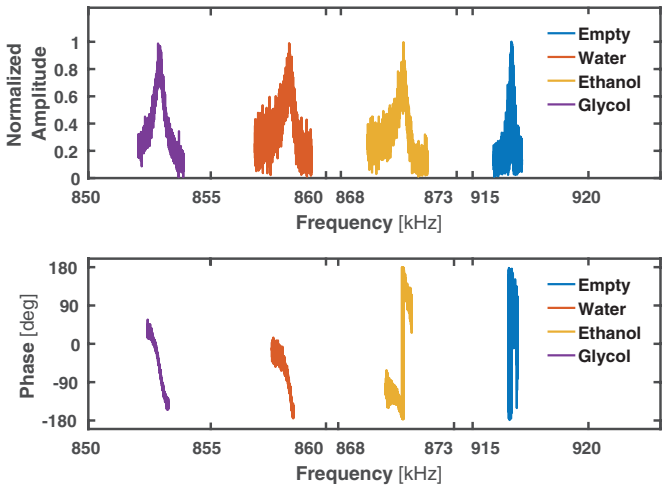

Figure A2. Normalized amplitude and phase (in degrees) responses near the resonance frequency of the first torsional mode for the empty hollow cantilever (blue) and the hollow cantilever filled with water (red), ethanol (yellow), and glycol (purple) at room temperature.

Appendix B. Effect of viscosity on quality factor

In order to provide quantitative energy dissipated due to the presence of fluid inside the channel, the quality factor due to fluid only is calculated following the formulation given Sader *et al* in [33]. The results are provided in table A1. The Q due to the fluid strongly depends on the nature of the fluid and on the

Table A1. Theoretically estimated quality factors for the first two flexural and the first torsional mode when the hollow cantilever is empty and filled with ethanol, water and glycol.

	First Flexural			Second Flexural			First Torsional		
	β	F(β)	Q_{fluid}	β	F(β)	Q_{fluid}	β	F(β)	Q_{fluid}
Air	0.26	148.96	6.9×10^9	1.62	3.43	1.6×10^8	1.72	—	—
Water	2.88	13.51	953768	17.83	0.37	26 081.7	19.72	—	—
Ethanol	4.57	8.57	4571714	28.29	0.28	15 761.7	31.29	—	—
Glycol	0.27	143.44	7.1×10^6	1.72	3.24	160182	1.9	—	—

Table A2. Resonance frequency for the first two flexural and the first torsional mode for three experiments. The SD is also reported.

		Ethanol		Water		Glycol	
Exp. N.	Mode	Freq (kHz)	SD	Freq (kHz)	SD	Freq (kHz)	SD
1	1st Flexural	126.423	0.019	123.950	0.050	123.002	0.039
2		126.461		124.007		122.989	
3		126.441		124.050		123.063	
1	2nd Flexural	777.529	0.078	764.635	0.259	759.123	0.067
2		777.685		764.848		759.257	
3		777.625		765.151		759.192	
1	1st Torsional	870.596	0.036	858.405	0.187	852.846	0.382
2		870.639		858.571		853.131	
3		870.660		858.729		853.508	

vibration mode. This is plotted against the Reynolds number β. This parameter, for each resonant mode ω_n, is defined by:

$$\beta_n = \frac{\rho \omega_n h_{fluid}^2}{\mu}, \tag{B.1}$$

where ρ and μ are the density and shear viscosity of the fluid with thickness h_{fluid}, respectively.

The quality factor due to the fluid is

$$Q_{fluid} = F(\beta_n) \frac{\rho_{cantilever}}{\rho} \left(\frac{h_{cantilever}}{h_{fluid}} \right) \left(\frac{b_{cantilever}}{b_{fluid}} \right) \left(\frac{L}{h_{fluid}} \right)^2 \tag{B.2}$$

where $F(\beta_n)$ is the normalized quality factors and expressed by:

$$F(\beta_n) = \frac{\beta_n}{16 \int_{-L_c}^{1} \int_{-1/2}^{1/2} |G(X,Z)|^2 \, dZdX}, \tag{B.3}$$

The channels of our device are considered to have neutral axis at the center, thus the function $G(X,Z)$ consists of only one term depending on the normalized deflection function of the cantilever beam and it does not account for asymmetric distribution of the inner channels (see [33] for further details).

Appendix C. Resonance frequencies for the different liquids

In order to show the accuracy and repeatability, in table A2 we report the values of the resonant frequencies for three separate experiments.

ORCID iDs

Urs Staufer https://orcid.org/0000-0002-3519-6467
Murali K Ghatkesar https://orcid.org/0000-0001-8423-3159

References

[1] Baskurt O K and Meiselman H J 2003 Blood rheology and hemodynamics *Seminars in Thrombosis and Hemostasis* **29** pp 435–50

[2] Dillon I G, Nelson P A and Swanson B S 1966 Measurement of densities and estimation of critical properties of the alkali metals *J. Chem. Phys.* **44** 4229–38

[3] Fadaei H, Scarff B and Sinton D 2011 Rapid microfluidics-based measurement of CO_2 diffusivity in bitumen *Energy & Fuels* **25** 4829–35

[4] Malkin A Y and Isayev A I 2017 *Rheology: Concepts, Methods and Applications* (Amsterdam: Elsevier)

[5] Vajjha R S and Das D K 2008 Measurements of specific heat and density of al 2 o 3 nanofluid *Conf. Proc.* (AIP) **1063** pp 361–70

[6] Martin S, Ricco A, Niemczyk T and Frye G 1989 Characterization of SH acoustic plate mode liquid sensors *Sensors Actuators* **20** 253–68

[7] Herrmann F, Hahn D and Büttgenbach S 1999 Separation of density and viscosity influence on liquid-loaded surface acoustic wave devices *Appl. Phys. Lett.* **74** 3410–12

[8] Liu Y, DiFoggio R, Sanderlin K, Perez L and Zhao J 2011 Measurement of density and viscosity of dodecane and decane with a piezoelectric tuning fork over 298–448 K and 0.1–137.9 MPa *Sensors and Actuators A: Physical* **167** 347–53

[9] Martin S, Frye G and Wessendorf K 1994 Sensing liquid properties with thickness-shear mode resonators *Sensors and Actuators A: Physical* **44** 209–18
[10] Mirea T, Olivares J, Clement M and Iborra E 2019 Impact of FBAR design on its sensitivity as in-liquid gravimetric sensor *Sensors Actuators* **289** 97–93
[11] Sparks D, Smith R, Cruz V, Tran N, Chimbayo A, Riley D and Najafi N 2009 Dynamic and kinematic viscosity measurements with a resonating microtube *Sensors Actuators* **149** 38–41
[12] Bircher B A, Krenger R and Braun T 2016 Automated high-throughput viscosity and density sensor using nanomechanical resonators *Sensors Actuators* **223** 784–90
[13] Monge R, Groenesteijn J, Alveringh D, Wiegerink R J, Lötters J and Fernandez L J 2017 SU–8 micro coriolis mass flow sensor *Sensors Actuators* **241** 744–9
[14] Sparks D, Smith R, Massoud-Ansari S and Najafi N 2004 Coriolis mass flow, density and temperature sensing with a single vacuum sealed mems chip *Solid-State Sensor, Actuator and Microsystems Workshop, Hilton Head Island, South Carolina* Citeseer **4**
[15] Belardinelli P, Hauzer L M F R, Šiškins M, Ghatkesar M K and Alijani F 2018 Modal analysis for density and anisotropic elasticity identification of adsorbates on microcantilevers *Appl. Phys. Lett.* **113** 143102
[16] Ghatkesar M K, Rakhmatullina E, Lang H-P, Gerber C, Hegner M and Braun T 2008 Multi-parameter microcantilever sensor for comprehensive characterization of newtonian fluids *Sensors Actuators* **135** 133–8
[17] Burg T P and Manalis S R 2003 Suspended microchannel resonators for biomolecular detection *Appl. Phys. Lett.* **83** 2698–700
[18] Sparks D, Smith R, Straayer M, Cripe J, Schneider R, Chimbayo A, Anasari S and Najafi N 2003 Measurement of density and chemical concentration using a microfluidic chip *Lab Chip* **3** 19–21
[19] Khan M, Schmid S, Larsen P, Davis Z, Yan W, Stenby E and Boisen A 2013 Online measurement of mass density and viscosity of pl fluid samples with suspended microchannel resonator *Sensors Actuators* **185** 456–61
[20] Belardinelli P, Ghatkesar M, Staufer U and Alijani F 2017 Linear and non-linear vibrations of fluid-filled hollow microcantilevers interacting with small particles *Int. J. Non-Linear Mech.* **93** 30–40
[21] Heuck F C 2010 *Developing and Analysing sub-10 μ Fluidic Systems with Integrated Electrodes for Pumping and Sensing in Nanotechnology Applications* PhD thesis
[22] Hug T, Biss T, de Rooij N and Staufer U 2005 Generic fabrication technology for transparent and suspended microfluidic and nanofluidic channels *Proc. of the 13th Int. Conf. on Solid-State Sensors, Actuators and Microsystems* **2** 11911194
[23] Ghatkesar M, Garza H, Heuck F and Staufer U 2014 Scanning probe microscope-based fluid dispensing *Micromachines* **5** 954–1001
[24] Rohlf J 1994 *Modern Physics From Alpha to Z0* (New York: Wiley)
[25] Lardies J and Gouttebroze S 2002 Identification of modal parameters using the wavelet transform *Int. J. Mech. Sci.* **44** 2263–83
[26] Newell W E 1968 Miniaturization of tuning forks *Science* **161** 1320–6
[27] Li M, Tang H X and Roukes M L 2007 Ultra-sensitive NEMS-based cantilevers for sensing, scanned probe and very high-frequency applications *Nat. Nanotechnol.* **2** 114
[28] Lee J, Shen W, Payer K, Burg T P and Manalis S R 2010 Toward attogram mass measurements in solution with suspended nanochannel resonators *Nano Lett.* **10** 2537–42
[29] Ghatkesar M K, Barwich V, Braun T, Ramseyer J-P, Gerber C, Hegner M, Lang H P, Drechsler U and Despont M 2007 Higher modes of vibration increase mass sensitivity in nanomechanical microcantilevers *Nanotechnology* **18** 445502
[30] Joshi S, Hung S and Vengallatore S 2014 Design strategies for controlling damping in micromechanical and nanomechanical resonators *EPJ Techniques and Instrumentation* **1** 5
[31] Schmid S, Villanueva L G, Roukes M L 2016 Quality factor *Fundamentals of Nanomechanical Resonators* (Berlin: Springer) pp 57–90
[32] Burg T P, Sader J E and Manalis S R 2009 Nonmonotonic energy dissipation in microfluidic resonators *Phys. Rev. Lett.* **102** 228103
[33] Sader J E, Lee J and Manalis S R 2010 Energy dissipation in microfluidic beam resonators: Dependence on mode number *J. Appl. Phys.* **108** 114507
[34] Lee J, Bryan A K and Manalis S R 2011 High precision particle mass sensing using microchannel resonators in the second vibration mode *Rev. Sci. Instrum.* **82** 023704